**Article:**
Hung, Shih-Hsuan and McKenna, Keith P. orcid.org/0000-0003-0975-3626 (2018) First-Principles Investigation of Titanium Nanoparticle Oxidation. Journal of Physical Chemistry C. pp. 3107-3114. ISSN 1932-7455

https://doi.org/10.1021/acs.jpcc.7b11582

# First Principles Investigation of Titanium Nanoparticle Oxidation

Shih-Hsuan Hung* and Keith P. McKenna*

*Department of Physics, University of York, Heslington, York YO10 5DD, United Kingdom.*

E-mail: sh1635@york.ac.uk; keith.mckenna@york.ac.uk

**Abstract**

We perform first-principles calculations to investigate the initial stages of titanium nanoparticle oxidation. We determine the most stable structure of a 181 atom decahedral nanoparticle with various oxygen coverages ranging from a single atom to full oxidation of the surface. Linear $O_{ad}$-Ti-$O_{ad}$ bonding configurations on the nanoparticle surface are found to be most stable for low oxygen coverage. The degree of lattice expansion is observed to gradually increase with increasing oxygen content up to 8.2 % for full oxidation of the surface. To investigate likely mechanisms for subsequent subsurface oxidation we calculate energy barriers for many inequivalent oxygen diffusion pathways. We find that the most favorable pathways involve penetration of oxygen into subsurface octahedral sites in the center of facets where the strain is largest. The results provide atomistic insight into the oxidation behavior of Ti nanoparticles and highlight the important role played by adsorption induced strain.

# 1 Introduction

Understanding how metallic nanoparticles oxidize is an important problem since in many applications they are exposed to an oxygen-rich environment (such as an ambient atmosphere, water or an oxide substrate).[1–3] There are differences between nanoparticle oxidation and the oxidation of bulk surfaces which are also of fundamental interest. In particular, the surface strain can play a much more significant role in nanoparticle oxidation due to the reduced symmetry and greater freedom for structural distortion. For example, scanning transmission electron microscopy (STEM) studies on the oxidation of Fe nanoparticles observed preferential oxidation in the center of facets due to the presence of a larger surface strain.[4] While surface oxidation of bulk metals has been well studied both experimentally and theoretically,[5,6] there have been far fewer investigations of nanoparticle oxidation.[7] In fact very little is known at the atomic level about the influence of strain on the oxidation of nanoparticles.

In this article, we employ first-principles theoretical approaches to investigate the initial stages of oxidation of a titanium nanoparticle. We consider Ti as a model system that is highly reactive to oxygen. Oxidized Ti nanoparticles also find important applications in photocatalysis, e.g. in self-cleaning glass and water splitting.[8–10] We show that adsorbed oxygen atoms preferentially form linear $O_{ad}$-Ti-$O_{ad}$ bonding configurations that involve two oxygen atoms bonded to one surface Ti atom. However, as the oxygen coverage on the surface increases, the stable configuration is modified to three adsorbed oxygen atoms sharing a single surface Ti atom. To provide insights into oxidation of the nanoparticle, we investigate the pathways for penetration of oxygen atoms from the surface to the sub-surface of the nanoparticle. We find that dilative strain on the nanoparticle surface due to the presence of adsorbed oxygen atoms facilitates the diffusion of oxygen atoms inside the nanoparticle. Oxygen atoms preferentially diffuse into the Ti nanoparticle in the center of facets where the dilative strain is largest. This investigation enhances the understanding of the oxidation of metallic nanoparticles, and also offers atomic insight into the interaction between oxygen atoms and the Ti nanoparticle surface.

The rest of the article is organized as follows. Sec. 2 discusses previous theoretical and experimental investigations on Ti nanoparticles and their oxidation. Sec. 3 details the methodology employed in our calculations. The results are presented in Sec. 4, the problems and challenges are discussed in Sec. 5 and our conclusions are summarized in Sec. 6.

## 2 Background

There have been numerous studies on the structure and properties of Ti nanoparticles. Guided ion beam mass spectrometry and photoelectron spectroscopy have shown that the morphology of Ti nanoparticles is icosahedral for $N \leq 130$ (where N is the number of atoms in the nanoparticle).[11,12] The structure and stability of small Ti nanoparticles in several morphologies have also been modeled using first-principles approaches with predictions in good

agreement with experimental results.[13–15] As the size of nanoparticles increases a transition to decahedral morphology is expected which has a lower strain than icosahedral.[16,17] Decahedral nanoparticles have five-fold symmetry and expose ten triangular close-packed facets. Decahedral morphologies are often observed experimentally for Ti nanoparticles up to the micrometer size.[18,19] For very large nanoparticles the bulk hcp structure should emerge as the most stable in order to minimize the strain in the nanoparticle core.[20]

We are not aware of any previous experimental study of the oxidation of Ti nanoparticles. However, oxidation of the Ti surface has been studied and provides constructive information. For example, an Auger electron spectroscopy (AES) and low-energy electron diffraction investigation of the single-crystal Ti(0001) surface revealed the formation of an ordered p(2 × 2) adatom superstructure at low oxygen coverage accompanied by modification of the work function.[21] X-ray photoelectron spectroscopy and ultraviolet photoemission spectroscopy studies have also demonstrated the appearance of a range of Ti oxidation states (from 2+ up to 4+) on oxidation of the surface depending on the conditions.[22–25] After the initial rapid surface oxidation, penetration of oxygen into bulk Ti is a much slower process due to the formation of a passivating oxide film.[24,26,27] However, AES studies have shown sub-surface diffusion of oxygen is significantly enhanced at temperatures above 500-700 K.[28,29] Despite these numerous investigations there is no unambiguous identification of the surface or sub-surface oxygen adsorption sites.

First-principles investigations into the interaction of oxygen with titanium have shown that oxygen incorporates into octahedral interstitial sites in bulk Ti.[30] At the Ti (0001) surface and close packed facets of small nanoparticles, oxygen is predicted to preferentially adsorb on threefold hollow sites.[6,7,31,32] Boureau *et al.* reported that if two oxygen atoms are located in adjacent adsorption sites there is a significant electronic density deformation preventing simultaneous occupation of adjacent hcp and fcc sites.[31] Energy barriers to oxygen diffusion in bulk Ti have also been calculated to be approximately 2.1 eV.[30] The majority of theoretical investigations on nanoparticles concentrate on small-sized nanoparticles with

icosahedral shape. Ti nanoparticles that contain either a single oxygen atom or a full monolayer of adsorbed oxygen have been considered.[7] However, a systematic study of nanoparticle oxidation with varying oxygen coverage is still missing.

# 3 Method

First-principles density functional theory (DFT) calculations are performed using the Perdew, Burke, and Ernzerhof (PBE) exchange-correlation potential[33] and a plane wave basis set as implemented in the Vienna ab initio simulation package (VASP).[34] The Brillouin zone (BZ) is sampled with the Monkhorst-Pack (MP) grid and the plane-wave basis set is truncated at an energy of 300 eV. The Γ-point is used for the BZ sampling of all nanoparticle calculations. Psuedopotentials include the following valence electrons: O ($2s^2$ $2p^4$) and Ti ($3d^3$ $4s^1$). The energy tolerance for self-consistent field optimization is $1\times10^{-4}$ eV. We employ the primitive unit cell for bulk Ti (hcp lattice) with a 7×7×7 MP grid used for BZ sampling. We use a 10×10×10 Å$^3$ supercell and Γ-point in MP grid sampling for optimization of the $O_2$ molecule. Following this approach, the calculated lattice constants of bulk Ti are $a$ =2.92 Å and $c/a$ =1.58, and the bond length of $O_2$ molecule is 1.29 Å, consistent with experiment.[35,36] To evaluate the stability of adsorbed oxygen, we calculate the average adsorption energy of oxygen atoms,

$$E_{\mathrm{ad}} = \frac{E_{\mathrm{oxi}} - E_{\mathrm{pure}}}{N_{\mathrm{O}}} - \frac{1}{2}E_{\mathrm{O_2}}, \tag{1}$$

where $E_{\mathrm{oxi}}$ is the total energy of the oxidized Ti nanoparticle, $E_{\mathrm{pure}}$ is the total energy of the bare Ti nanoparticle, $N_{\mathrm{O}}$ is the number of adsorbed oxygen atom, and $E_{\mathrm{O_2}}$ is the total energy of an isolated $O_2$ molecule. To analyze the strain contributions to the adsorption energy we also calculate the strain energy,

$$E_{\mathrm{strain}} = E'_{\mathrm{oxi}} - E_{\mathrm{pure}}, \tag{2}$$

where $E'_{\text{oxi}}$ is the total energy of a bare Ti nanoparticle but in the optimized geometry corresponding to the oxidized nanoparticle. In this way $E_{\text{strain}}$ characterizes the strain energy cost to distort the nanoparticle into the oxidized geometry.

To model the diffusion of an oxygen atom from the surface to the sub-surface of the nanoparticle we employ a constrained optimization approach. The initial position of a series of images along the diffusion pathway are obtain by linear interpolation between the initial ($\mathbf{R}_i$) and final structures ($\mathbf{R}_f$),

$$\mathbf{R}(\mathbf{t}) = (1-t)\mathbf{R}_i + t\mathbf{R}_f, \tag{3}$$

where $t$ is an interpolation parameter ranging from 0 to 1 that controls the position of the diffusing oxygen atom. The total energy of each image is minimized with respect to relaxation of all atoms within a given radius of the diffusing oxygen atom (with the diffusing atom held fixed). This approach is adopted to allow us to focus on the barrier to diffusion for a single oxygen atom. If unconstrained optimization is employed oxygen diffusion can trigger displacement of remote oxygen ions which complicates the analysis. We tested a range of constraint radii from 2 to 7 Å and find 4 Å provides a good compromise between capturing local distortions associated with oxygen diffusion while minimizing effects on oxygen ions further away. The interpolation is performed using the VASP Transition State Tools (VTST) script.[37]

# 4 Results

## 4.1 Adsorption of oxygen on the titanium (0001) surface and nanoparticle

We consider a 181-atom Ti nanoparticle with the decahedral morphology for the investigation of oxidation as illustrated in Fig. 1a (hereafter $\text{Dh}_{181}$). There are several reasons for selecting

this nanoparticle as the focus for our study. Firstly, decahedral morphologies are commonly observed experimentally.[38–40] Secondly, it is necessary to model a sufficiently large nanoparticle to correctly capture the interplay between oxygen adsorption, nanoparticle strain and oxygen diffusion. The $Dh_{181}$ is larger than that considered in any previous studies, but small enough to be computationally feasible.[41,42] The calculated formation energy with respect to bulk Ti is 0.81 eV per atom.

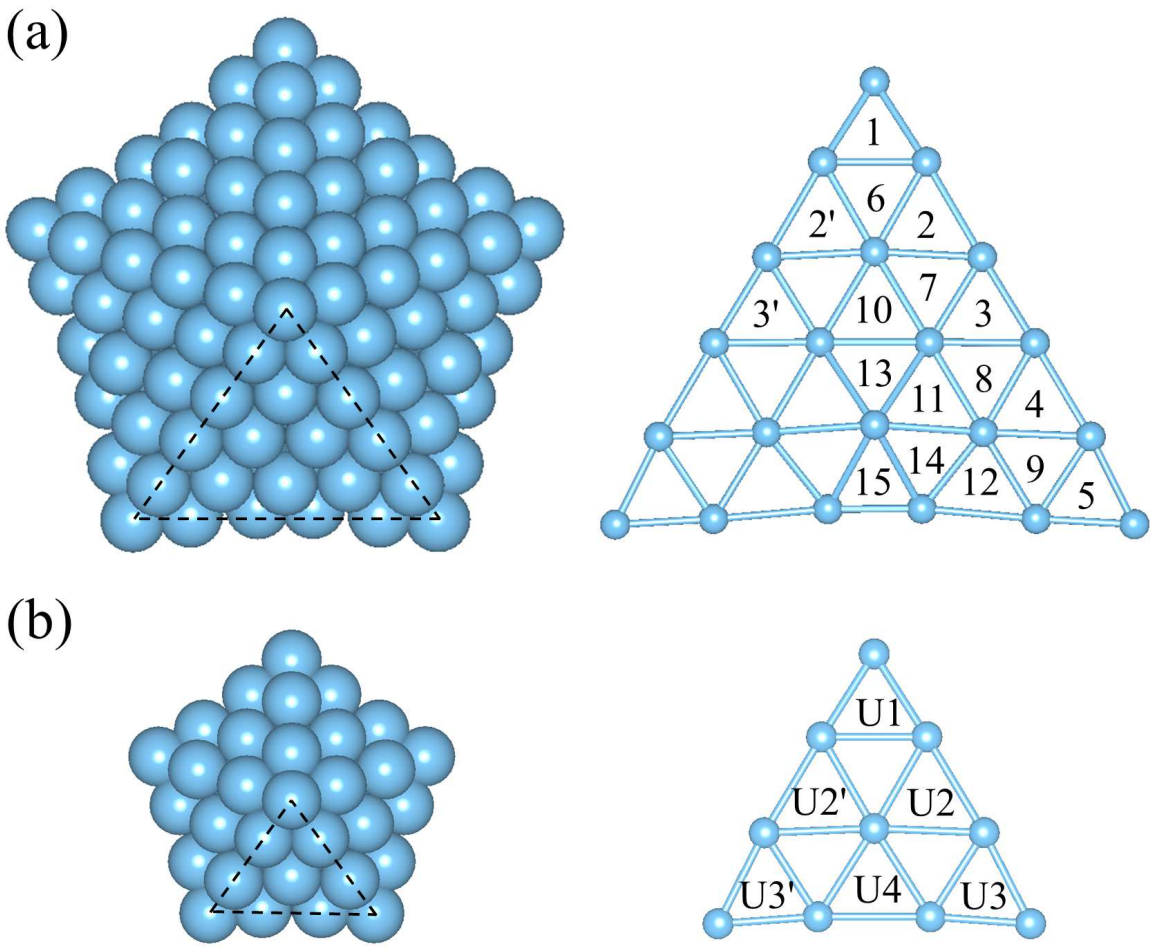


Figure 1: The figures on the left shows the top view of the surface (a) and subsurface (b) of the $Dh_{181}$ Ti nanoparticle (Ti atoms represented by blue spheres). The figures on the right are partial enlargements of the surface and sub-surface facets (see dashed triangles). The inequivalent adsorption hollow sites are labeled 1 to 15 for the surface and U1 to U4 for the subsurface. The primed sites are adsorption sites that are equivalent by mirror symmetry.

In order to provide insight into the chemical interaction between oxygen and titanium, we

first consider the simpler case of oxygen adsorption on the $\alpha$-Ti (0001) surface. The (0001) surface is considerably simpler as compared to the nanoparticle, since it only possesses two inequivalent oxygen adsorption sites (the fcc and hcp threefold hollow sites, see Fig. S1 in Supporting Information). The supercell employed to model the surface consists of an eight monolayer Ti slab with the dimensions $x = y = 17.6$ Å and $z = 36$ Å and a 5×5×1 MP grid is utilized for BZ sampling. The difference between hcp and fcc adsorption sites is that the former contains a Ti atom located directly below the adsorption site in the sub-surface layer, whereas the latter does not. The adsorption energies for a single oxygen atom on the Ti(0001) surface are -5.67 and -6.08 eV for the hcp and fcc sites respectively (a difference of 0.41 eV). To understand the origin of this difference in stability, we have calculated the strain energy associated with oxygen adsorption (see Sec. 3). The strain energy for adsorption on the hcp site is 0.17 eV greater than that for the fcc site, partly explaining the difference in the adsorption energies. Bader analysis of the electron density suggests that the preference for the fcc adsorption site is also driven partially by electrostatics. For both adsorption sites, the oxygen atom acquires a negative charge due to the transfer of electrons from the surrounding Ti atoms. The oxygen atom has three neighboring Ti atoms for both hcp and fcc sites. However, the fcc site contains three positively charged second nearest neighbor Ti atoms while the hcp site has only a single one. Therefore, oxygen adsorption on the fcc site benefits from the additional attractive electrostatic interactions that increases its stability. These results indicate that both strain energy and electrostatics play important roles in the adsorption of oxygen on the Ti(0001) surface. We also calculated the same interaction with the fcc Ti(111) surface finding very similar results.

The above results indicate that oxygen adsorption takes place on three-fold hollow sites on titanium, with the fcc site being the most stable. The $Dh_{181}$ nanoparticle presents 15 inequivalent threefold hollow sites (including fcc and hcp sites) as shown in Fig. 1a. We calculate the adsorption energy for an oxygen atom on each of these sites. Table 1 shows the adsorption energy and strain energy for each oxygen adsorption site on the nanoparticle

surface. Site 7 has the most stable configuration for a single oxygen atom ($E_{ad}$=-5.96). An oxygen atom on this fcc site (which is more stable than hcp) also has the smallest strain energy (0.11 eV). Site 1 is the most unfavorable adsorption configuration ($E_{ad}$=-5.46) and is an hcp site in line with expectations. As for the Ti(0001) surface, we found a correlation between high strain energies and low adsorption energies. However, again as for the surface, electrostatic interactions also play a role in determining the relative stability of different sites on the nanoparticle.

**Table 1: Adsorption energy and strain energy for single oxygen atoms adsorbed on the surface and subsurface layers of the $Dh_{181}Ti$ nanoparticle (see Fig. 1 for definition of the adsorption sites).**

| Index | Site | $E_{ad}$ (eV) | $E_{strain}$ (eV) |
|---|---|---|---|
| 1 | hcp | -5.47 | 0.16 |
| 2 | hcp | -5.86 | 0.19 |
| 3 | hcp | -5.81 | 0.15 |
| 4 | hcp | -5.76 | 0.18 |
| 5 | hcp | -5.76 | 0.17 |
| 6 | fcc | -5.65 | 0.21 |
| 7 | fcc | -5.96 | 0.11 |
| 8 | fcc | -5.67 | 0.26 |
| 9 | fcc | -5.68 | 0.22 |
| 10 | hcp | -5.65 | 0.37 |
| 11 | hcp | -5.83 | 0.17 |
| 12 | hcp | -5.65 | 0.27 |
| 13 | fcc | -5.89 | 0.18 |
| 14 | fcc | -5.51 | 0.24 |
| 15 | hcp | -5.49 | 0.35 |
| U1 | oct | -5.82 | 0.13 |
| U2 | oct | -5.55 | 0.22 |
| U3 | oct | -5.62 | 0.21 |
| U4 | oct | -5.38 | 0.36 |

We also calculated the adsorption energy for an oxygen atom in the sub-surface layer to evaluate the preference for an oxygen atom to penetrate into the nanoparticle. We find oxygen atoms prefer to incorporate into octahedral (oct) interstitial sites of nanoparticles as shown in Fig. 1b (labeled U1 to U4). Table 1 summarizes the adsorption energies and strain energies for these sub-surface oxygen sites. Site U1 is found to be the most stable

and also has the lower strain energy (0.13 eV) in comparison to other sub-surface oxygen sites. However, the most stable sub-surface site is 0.14 eV less stable than the most stable surface site. The result indicates that the preferential adsorption site of an oxygen atom is on the surface fcc hollow sites. This is due to the smaller strain energy and the favorable electrostatic interactions. These findings are consistent with recent work which investigated the interaction between oxygen atoms and Pt-Cu core/shell nanoparticles.[43]

## 4.2 Most stable oxidized nanoparticle and lattice expansion

In order to investigate increasing oxygen coverage on the surface of the nanoparticle, we first arrange pairs of oxygen atoms on one of the facets and determine the lowest energy configurations. The systematic study reveals that the most stable adsorption energies of one, two, and three pairs of oxygen atoms are -5.99, -6.05 and -5.97 eV per oxygen atom respectively. The structures are shown in Fig. 2a-c. In these three structures, the most stable configurations invariably constitute a linear $O_{ad}$-Ti-$O_{ad}$ structure. The stability of the $O_{ad}$-Ti-$O_{ad}$ configuration is a result of maximizing the $O_{ad}$-$O_{ad}$ distance. As the coverage increases it becomes impossible to accommodate any more linear $O_{ad}$-Ti-$O_{ad}$ structures on the surface. In this case the most stable oxygen configuration transforms into a configuration where surface Ti atoms are bonded to three adsorbed oxygen atom in a triangular structure, as shown in Fig. 2d. This transformation makes more adsorption sites available on the surface and further prevents oxygen atoms from occupying the adjacent hcp and fcc adsorption sites simultaneously.

We calculated the total energies of several oxidized $Dh_{181}$ nanoparticles to compare their stability and determine the energetically stable structures for different oxygen coverages. We consider 20, 40, 60, 80, 100, and 150 oxygen atoms adsorbing on the $Dh_{181}$ nanoparticle. For each coverage, we calculate 4, 11, 8, 4, 5 and 1 different oxygen configuration(s). The oxygen atoms are distributed equally over all facets (for example, each facet has 2 oxygen atoms for 20 adsorbed oxygen atoms). The calculations always employ an even number

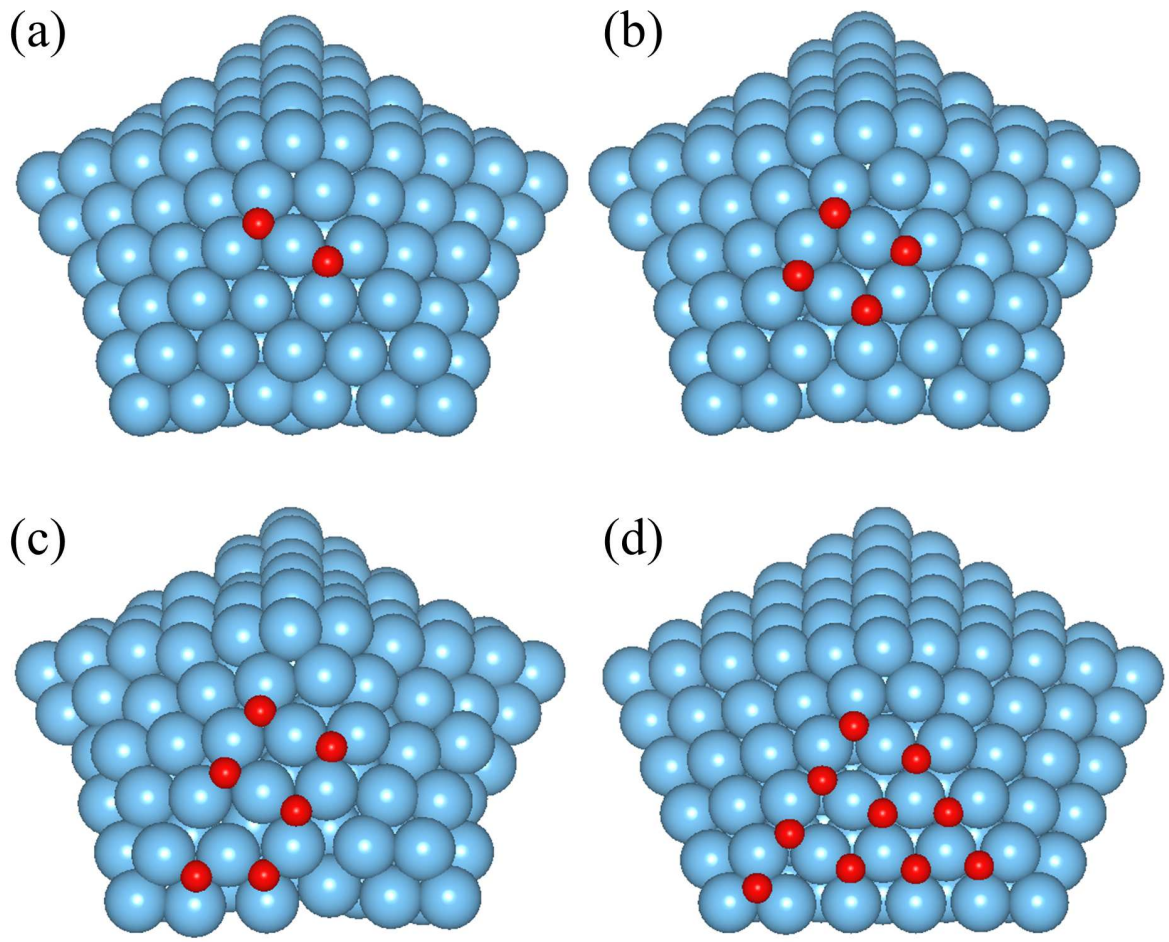


Figure 2: (a), (b) and (c) show the lowest energy configuration for one, two and three pairs of oxygen atoms absorbed on a facet. (d) shows an example structure where three oxygen atoms share a single surface Ti atom. The blue and red spheres represent titanium and oxygen atoms respectively.

of adsorbed oxygen atoms corresponding to the adsorption and dissociation of an integer number of oxygen molecules.[44] The most energetically favorable structure of oxidized Ti nanoparticles with 20 to 150 adsorbed oxygen atoms on the surface are shown in Fig. 3. In the following these structures are denoted as C20 to C150. The point group symmetries for C20 to C80, C100, and C150 are $C_{5h}$, $D_5$ and $D_{5h}$, respectively.[42,45] The average adsorption energies of C20, C40, C60, C80, C100, and C150 are -5.79, -5.84, -5.88, -5.81, -5.75, and -5.48 eV per oxygen atom. The most stable adsorption energy is observed at C60 (Fig. 3c) since this oxidized configuration maximizes the number of linear $O_{ad}$-Ti-$O_{ad}$ structures on the surface. A phase diagram indicating the oxygen chemical potential range in which these different structures are stable is shown in Fig. S2 in Supporting Information.

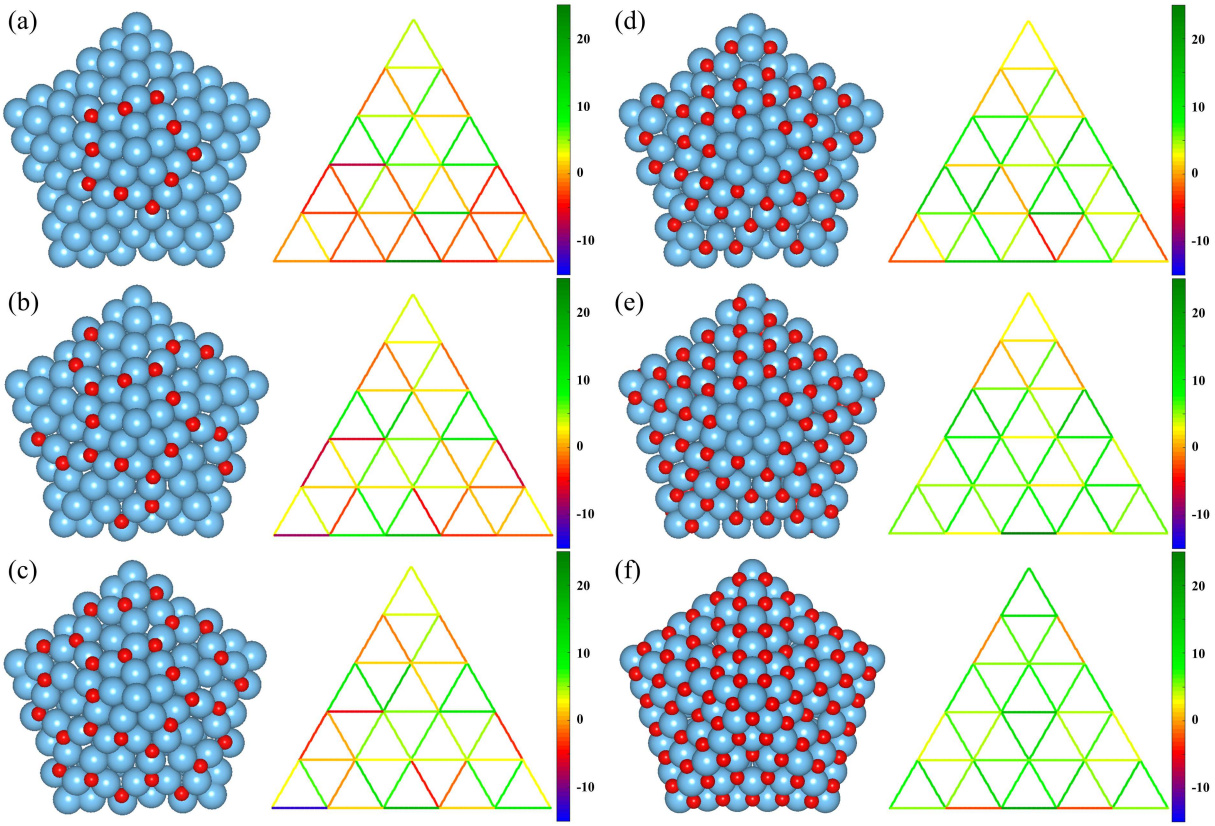


Figure 3: The structures (figures on the left) and surface strain (figures on the right) of (a) C20, (b) C40, (c) C60, (d) C80 (e) C100 and (f) C150 nanoparticle structures. The triangular grids are the Ti-Ti bonds on the surface and the color of the bonds represent the value of the strain relative to the pristine Ti nanoparticle.

The calculated average Ti-Ti bond length on the surface is increased from 2.87 to 3.03 Å as the number of oxygen atoms is increased from 20 to 150. In order to assess the Ti-Ti bond distortion with respect to variation of oxygen coverage, we calculate the strain of each oxidized nanoparticle relative to the pure nanoparticle (panels on the right in Fig. 3) The results indicate that some surface bonds in the Ti nanoparticle are expanded and others contracted in the C20, C40, C60, and C80 structures. However almost every bond on the surface of the C100 and C150 structures are expanded. The average strain of the surface Ti-Ti bonds for C20 to C150 are 2.0, 2.5, 3.7, 5.6, 6.5, and 8.2 %.

## 4.3 Oxygen diffusion on the Ti nanoparticle

To achieve further oxidation of $Dh_{181}$ nanoparticle, there are two possible scenarios. First, the Ti atoms may diffuse out of the nanoparticle forming an inner void.[46] Alternatively oxygen atoms may diffuse into the nanoparticle and incorporate into octahedral interstitial sites. To examine the former situation, we optimized the oxidized nanoparticles with one Ti atom relocated from the surface to on top of the adsorbed oxygen atoms (in the three fold hollow, bridge and top sites). The configurations with an outward displaced Ti atom are always found to be energetically unfavorable relative to the original one. This suggests that Ti atoms do not have a strong tendency to diffuse to the outer surface to allow further oxidation.

Next, we calculated the energy barriers of many different pathways to assess the possibility of oxygen diffusion from the surface to sub-surface of $Dh_{181}$ nanoparticle. We only consider diffusion pathways that result in a final configuration that is more stable than the original. Systematic investigation reveals that penetration of oxygen in the C20, C40, and C60 structures always increases the energy indicating they are locally stable against further oxidation. However, for C80 and C100 a number of structures with oxygen displaced from the surface into the subsurface present a higher stability. The possible diffusion pathways that reduce the total energy are described as follows. Referring to Fig. 1 for the definition

of the sites, the C80 structure has the following pathways: (A) 8 $\rightarrow$ U3 and (B) 13 $\rightarrow$ U4. Pathways for the C100 structure are: (A) 8 $\rightarrow$ U3, (B) 13 $\rightarrow$ U4, (C) $2' \rightarrow$ U$2'$ and (D) $3' \rightarrow$ U$3'$. These pathways are shown in Fig. 4. The smallest energy barriers to oxygen diffusion in the C80 and C100 structures are 1.50 and 1.21 eV respectively. Both of them belong to path-B (see Fig. 4) indicating that oxygen preferentially diffuses into the nanoparticle in the middle of the facets. We do not show the oxygen diffusion pathways for the C150 structure since displacement of an oxygen into to the subsurface region followed by structural optimization results in several surface oxygen ions incorporating into subsurface sites. This makes it difficult to identify energy barriers for individual oxygen atom diffusion processes. However, this observation suggests that the high coverage C150 structure is quite unstable and the penetration of oxygen atoms into the subsurface layer is promoted.

The results presented above demonstrate that the energy barrier to diffusion of oxygen ions from the surface to the subsurface decreases with increasing oxygen coverage. It was also shown in Sec. 4.2 that the Ti bonds progressively expand with increasing oxygen coverage suggesting a possible explanation for the effect. Indeed when we calculate the energy barrier to oxygen penetration in the center of the facet for structures C20 to C100 we see a very clear correlation with the average surface strain (Fig. 5). An increase of 1 % in the surface strain is shown to decrease the energy barrier to oxygen diffusion by around 0.1 eV. One can make a simple estimate for the rate of oxygen penetration using these calculated energy barriers.[30] For example using the Arrhenius equation with a typical vibrational frequency prefactor of $10^{13}$ Hz we estimate a relatively high diffusion rate of 0.2 Hz can be achieved at temperatures as low as 700 K for the C100 structure. These results highlight the importance of surface strain in controlling the oxidation of Ti nanoparticles.

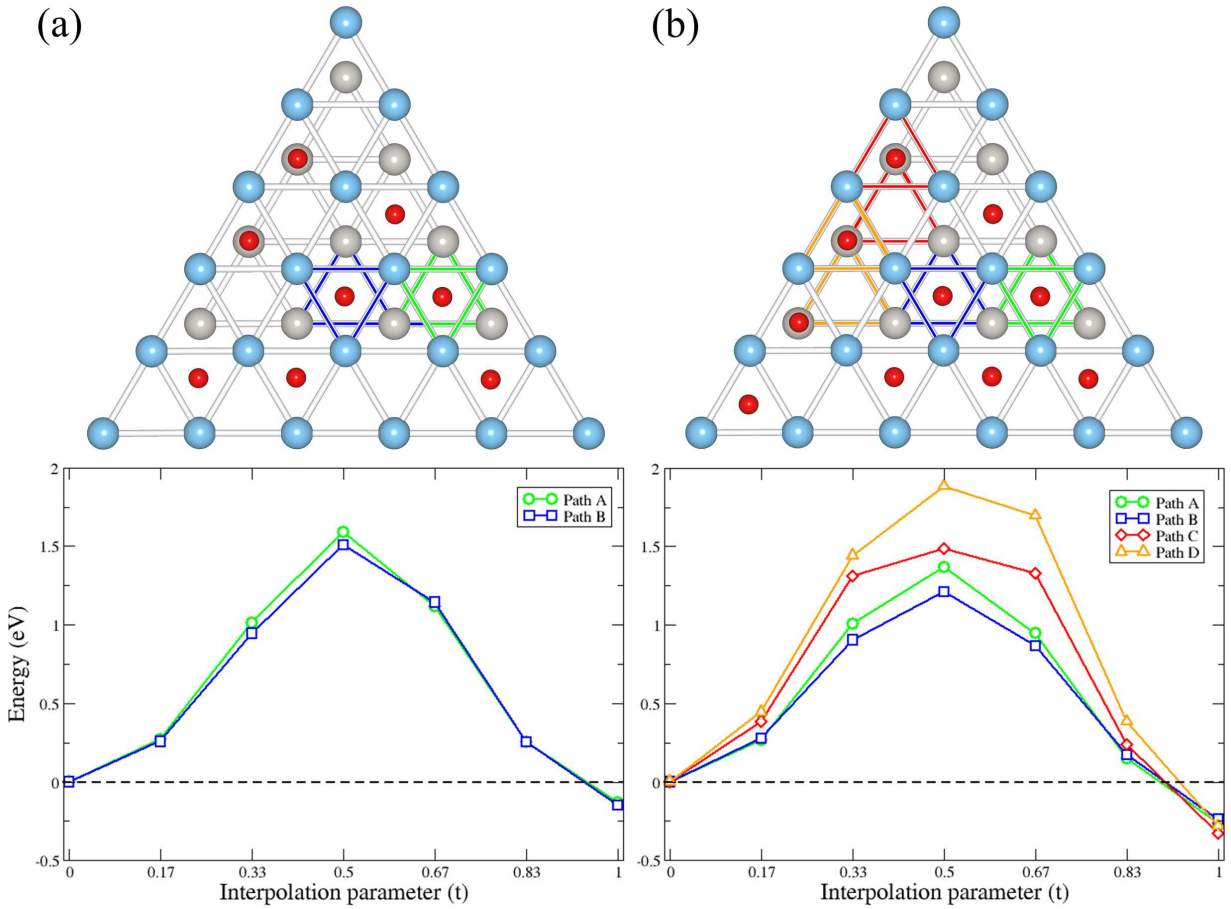


Figure 4: Oxygen atom diffusion pathways (top panels) and the respective energy barriers (bottom panels) on (a) C80 and (b) C100 nanoparticle structures. Surface and sub-surface Ti atoms are represented as blue and gray spheres and oxygen atoms as red spheres. The triangles highlight the start- and end-points for the diffusion pathways A-D (see legend in lower panel).

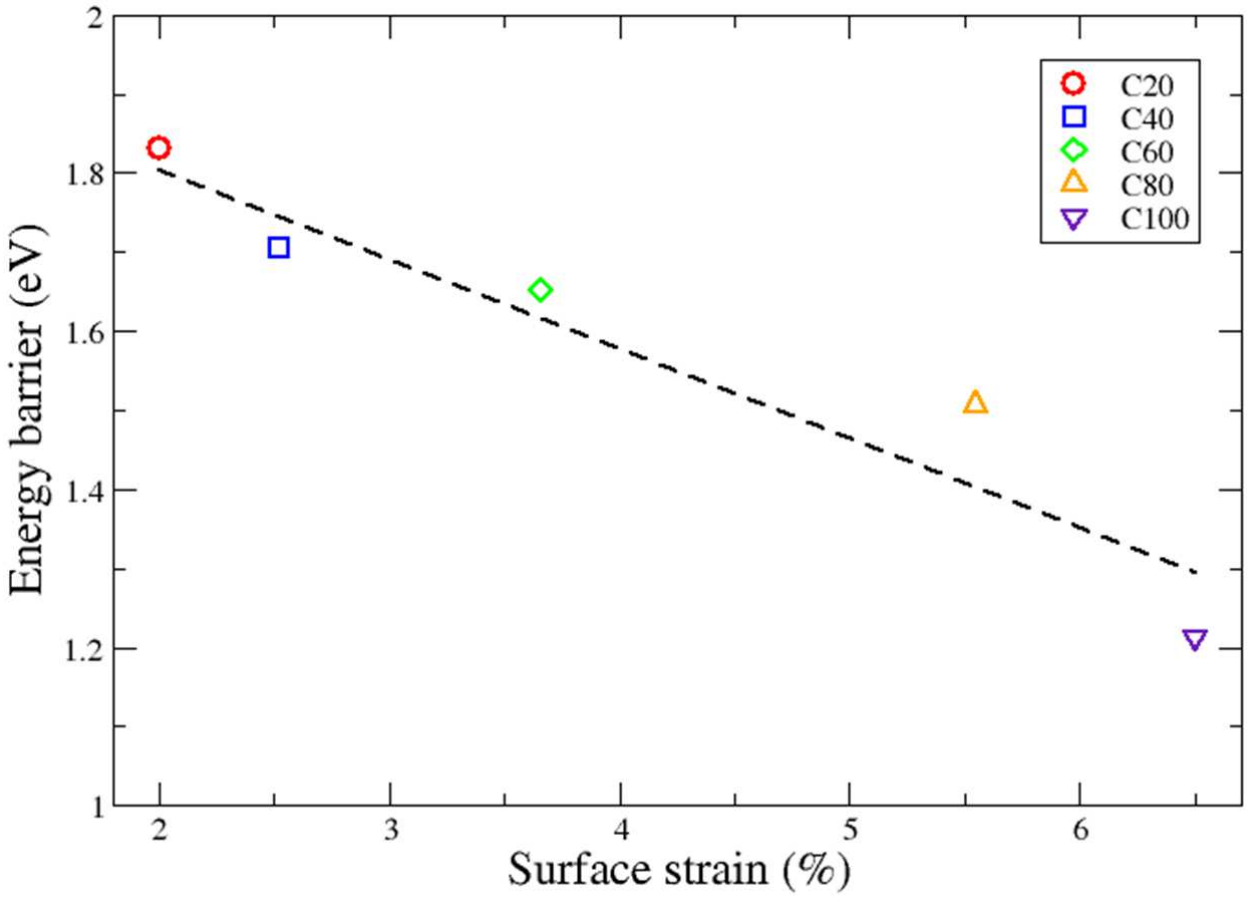


Figure 5: The variation of the barrier to penetration of oxygen from the surface to the subsurface (in the center of the facet) with respect to the average surface Ti-Ti bond strain. The dashed line is a guide to the eye highlighting the strong linear correlation.

# 5 Discussion

Several factors may influence the accuracy of the results presented above. First we consider the choice of the exchange-correlation potential in the DFT calculations. The PBE functional is known to provide a good description for bulk Ti properties, predicted Ti-O bond lengths and the formation enthalpy of bulk $TiO_2$.[47–49] It is well known PBE underestimates the band gap of $TiO_2$, but this should not affect the predictions of oxygen adsorption energies and diffusion barriers presented in this paper. Therefore, we believe that the choice of PBE is reasonable for this investigation.

The most stable structures of oxidized nanoparticles are obtained through a systematic investigation of different high symmetry configurations. We note that real nanoparticles may exhibit patterns of oxygen atom adsorption with a much lower symmetry. However, it would not be computationally feasible to investigate all possible adsorption configurations at the DFT level. The approach we employ allows us to systematically investigate trends with respect to increasing oxygen coverage for reasonable oxygen configurations. First principles molecular dynamics (MD) could be an alternative approach to access lower symmetry configurations but is extremely computationally challenging owing to the large number of atoms and the long timescales needed for equilibration.

To allow comparison to previous theoretical studies of the penetration of adsorbed oxygen into Ti(0001) surface we also calculate the barrier to diffusion of a single adsorbed oxygen in the center of a facet obtaining 1.56 eV. This is comparable to the barrier obtained for the Ti(0001) surface (1.55 eV).[50] However, there is a very different trend with increasing oxygen coverage between the nanoparticle and the extended surface. As discussed in Sec. 4.3, for the nanoparticle the barrier progressively decreases with increasing oxygen coverage due to the lattice expansion. However, for the Ti(0001) surface the barrier reaches a minimum value at 25% oxygen coverage and a maximum at 75% .[50] This different behavior is due to the lower symmetry of the nanoparticle and the development of more complex strain fields on oxygen adsorption. In particular, the strong interaction between oxygen and low-coordinated Ti

atoms (edge and vertex atoms) on the nanoparticles drives expansion of Ti-Ti bonds in the facets facilitating more facile penetration of oxygen into the subsurface layer.

We are not aware of any experimental studies of Ti nanoparticle oxidation to which we could compare our results. However, we note that the prediction of anisotropic penetration of oxygen into metallic nanoparticles driven by strain fields has been observed in a STEM study of the oxidation of iron nanoparticles.[4] This suggests that the trends discussed in this paper may apply more generally to the oxidation of highly reactive metals.

# 6 Conclusion

In summary, we have investigated the structure and stability of $Dh_{181}$ Ti nanoparticles with respect to variation of the oxygen coverage using first-principles methods. We have also investigated how the penetration of oxygen into the subsurface region, corresponding to the initial stages of nanoparticle oxidation, is influenced by lattice strain. We show that the strain energy plays a dominant role in the reaction between oxygen atoms and the Ti nanoparticle. Linear $O_{ad}$-Ti-$O_{ad}$ structures are shown to be most stable for low oxygen coverages. As the oxygen coverage increases there is a progressive expansion of Ti-Ti bonds on the nanoparticle facets reaching over 8% for full monolayer coverage. The most favorable pathway for subsequent oxidation is through the penetration of oxygen from the surface to subsurface interstitial sites at the center of the facets. The associated barrier to diffusion decreases from 1.83 to 1.21 eV as the surface oxygen coverage increases showing a nearly linear correlation with the average surface strain. This behavior is different to that predicted for the extended Ti(0001) surface due to the lower symmetry of the nanoparticle and the development of more complex strain fields on oxygen adsorption. Overall, this paper provides atomistic insight into the oxidation of Ti nanoparticles and highlights the important role played by dilative strain in facilitating oxygen diffusion into the nanoparticle core.

# 7 Acknowledgments

K.P.M. acknowledges support from EPSRC (EP/K003151/1 and EP/P006051/1). This work made use of the facilities of Archer, the UK's national high-performance computing service, via our membership in the UK HPC Materials Chemistry Consortium, which is funded by EPSRC (EP/L000202/1). This work also made use of the facilities of N8 HPC Centre of Excellence, provided and funded by the N8 consortium and EPSRC (EP/K000225/1). The Centre is coordinated by the Universities of Leeds and Manchester. All data created during this research are available by request from the University of York Research database http://dx.doi.org/TBC.

# References

(1) Lok, C.-N.; Ho, C.-M.; Chen, R.; He, Q.-Y.; Yu, W.-Y.; Sun, H.; Tam, P. K.-H.; Chiu, J.-F.; Che, C.-M. Silver nanoparticles: partial oxidation and antibacterial activities. *J. Biol. Inorg. Chem.* **2007**, *12*, 527–534.

(2) Schalow, T.; Laurin, M.; Brandt, B.; Schauermann, S.; Guimond, S.; Kuhlenbeck, H.; Starr, D. E.; Shaikhutdinov, S. K.; Libuda, J.; Freund, H.-J. Oxygen storage at the metal/oxide interface of catalyst nanoparticles. *Angew. Chem. Int. Ed.* **2005**, *44*, 7601–7605.

(3) Reier, T.; Oezaslan, M.; Strasser, P. Electrocatalytic oxygen evolution reaction (OER) on Ru, Ir, and Pt catalysts: A comparative study of nanoparticles and bulk materials. *ACS Catalysis* **2012**, *2*, 1765–1772.

(4) Pratt, A.; Lari, L.; Hovorka, O.; Shah, A.; Woffinden, C.; Tear, S. P.; Binns, C.; Kröger, R. Enhanced oxidation of nanoparticles through strain-mediated ionic transport. *Nat. Mater.* **2014**, *13*, 26–30.

(5) Kofstad, P.; Anderson, P.; Krudtaa, O. Oxidation of titanium in the temperature range 800–1200 ° C. *J. Less-Common Met.* **1961**, *3*, 89–97.

(6) Schneider, J.; Ciacchi, L. C. First principles and classical modeling of the oxidized titanium (0001) surface. *Surf. Sci.* **2010**, *604*, 1105–1115.

(7) Chibisov, A. Oxygen adsorption on small Ti clusters: A first-principles study. *Comput. Mater. Sci.* **2014**, *82*, 131–133.

(8) Jang, J. S.; Kim, H. G.; Joshi, U. A.; Jang, J. W.; Lee, J. S. Fabrication of CdS nanowires decorated with $TiO_2$ nanoparticles for photocatalytic hydrogen production under visible light irradiation. *Int. J. Hydrogen Energy* **2008**, *33*, 5975–5980.

(9) Jennings, P. C.; Pollet, B. G.; Johnston, R. L. Theoretical studies of Pt–Ti nanoparticles for potential use as PEMFC electrocatalysts. *Phys. Chem. Chem. Phys.* **2012**, *14*, 3134–3139.

(10) Blackmore, C. E.; Rees, N. V.; Palmer, R. E. Modular construction of size-selected multiple-core Pt–$TiO_2$ nanoclusters for electro-catalysis. *Phys. Chem. Chem. Phys.* **2015**, *17*, 28005–28009.

(11) Lian, L.; Su, C.-X.; Armentrout, P. B. Collision-induced dissociation of $Ti_n^+$ ($n$ = 2–22) with Xe: Bond energies, geometric structures, and dissociation pathways. *J. Chem. Phys.* **1992**, *97*, 4084–4093.

(12) Liu, S.-R.; Zhai, H.-J.; Castro, M.; Wang, L.-S. Photoelectron spectroscopy of $Ti_n^-$ clusters ($n$ = 1–130). *J. Chem. Phys.* **2003**, *118*, 2108–2115.

(13) Wang, S.-Y.; Duan, W.; Zhao, D.-L.; Wang, C.-Y. First-principles study of the stability of the icosahedral $Ti_{13}$, $Ti_{13}^{-1}$, and $Ti_{13}^{+1}$ clusters. *Phys. Rev. B* **2002**, *65*, 165424.

(14) Wang, S.-Y.; Yu, J.-Z.; Mizuseki, H.; Yan, J.-A.; Kawazoe, Y.; Wang, C.-Y. First-principles study of the electronic structures of icosahedral $Ti_N$ ($N$ = 13, 19, 43, 55) clusters. *J. Chem. Phys.* **2004**, *120*, 8463–8468.

(15) Castro, M.; Liu, S.-R.; Zhai, H.-J.; Wang, L.-S. Structural and electronic properties of small titanium clusters: A density functional theory and anion photoelectron spectroscopy study. *J. Chem. Phys.* **2003**, *118*, 2116–2123.

(16) Baletto, F.; Ferrando, R. Structural properties of nanoclusters: Energetic, thermodynamic, and kinetic effects. *Rev. Mod. Phys.* **2005**, *77*, 371–423.

(17) Cleveland, C. L.; Landman, U. The energetics and structure of nickel clusters : Size dependence. *J. Chem. Phys.* **1991**, *94*, 7376–7396.

(18) Zhang, W.; Liu, Y.; Cao, R.; Li, Z.; Zhang, Y.; Tang, Y.; Fan, K. Synergy between crystal strain and surface energy in morphological evolution of five-fold-twinned silver crystals. *J. Am. Chem. Soc.* **2008**, *130*, 15581–15588.

(19) Elechiguerra, J. L.; Reyes-Gasga, J.; Yacaman, M. J. The role of twinning in shape evolution of anisotropic noble metal nanostructures. *J. Mater. Chem.* **2006**, *16*, 3906–3919.

(20) Patala, S.; Marks, L. D.; Olvera de la Cruz, M. Elastic strain energy effects in faceted decahedral nanoparticles. *J. Phys. Chem. C* **2013**, *117*, 1485–1494.

(21) Jonker, B. T.; Morar, J. F.; Park, R. L. Surface states and oxygen chemisorption on Ti(0001). *Phys. Rev. B* **1981**, *24*, 2951–2957.

(22) Hagsteöm, A.; Platau, A.; Kaelsson, S.-E. Adsorption of oxygen at room temperature on polycrystalline titanium studied by ultraviolet and X-ray photoelectron spectroscopy. *phys. stat. solidi (b)* **1977**, *83*, 77–84.

(23) Hanson, D. M.; Stockbauer, R.; Madey, T. E. Photon-stimulated desorption and other spectroscopic studies of the interaction of oxygen with a titanium (001) surface. *Phys. Rev. B* **1981**, *24*, 5513–5521.

(24) Lu, G.; Bernasek, S. L.; Schwartz, J. Oxidation of a polycrystalline titanium surface by oxygen and water. *Surf. Sci.* **2000**, *458*, 80–90.

(25) Carley, A. F.; Chalker, P. R.; Riviere, J. C.; Roberts, M. W. The identification and characterisation of mixed oxidation states at oxidised titanium surfaces by analysis of X-ray photoelectron spectra. *J. Chem. Soc., Faraday Trans. 1* **1987**, *83*, 351–370.

(26) Martin, M.; Mader, W.; Fromm, E. Oxidation of iron, aluminium and titanium films in the temperature range 50–200 ° C. *Thin Solid Films* **1994**, *250*, 61–66.

(27) Bignolas, J.; Bujor, M.; Bardolle, J. A study of the early stages of the kinetics of titanium oxidation by Auger electron spectroscopy and mirror electron microscopy. *Surf. Sci. Lett.* **1981**, *108*, L453–L459.

(28) Vaquila, I.; Passeggi, M. C. G.; Ferrón, J. Oxidation process in titanium thin films. *Phys. Rev. B* **1997**, *55*, 13925–13931.

(29) Takakuwa, Y.; Ishidzuka, S.; Yoshigoe, A.; Teraoka, Y.; Yamauchi, Y.; Mizuno, Y.; Tonda, H.; Homma, T. Real-time monitoring of oxidation on the Ti (0 0 0 1) surface by synchrotron radiation photoelectron spectroscopy and RHEED–AES. *Appl. Surf. Sci.* **2003**, *216*, 395–401.

(30) Wu, H. H.; Trinkle, D. R. Direct diffusion through interpenetrating networks: Oxygen in titanium. *Phys. Rev. Lett.* **2011**, *107*, 045504.

(31) Boureau, G.; Capron, N.; Tétot, R. A first-principles study of dilute solutions of oxygen in titanium. *Scr. Mater.* **2008**, *59*, 1255–1258.

(32) S-Y. Liu, Y.-S. Z., F-H. Wang; Shang, J.-X. Ab initio study of oxygen adsorption on the Ti(0001) surface. *J. Phys.: Condens. Matter* **2007**, *19*, 226004.

(33) Perdew, J. P.; Burke, K.; Ernzerhof, M. Generalized gradient approximation made simple. *Phys. Rev. Lett.* **1996**, *77*, 3865–3868.

(34) Kresse, G.; Furthmüller, J. Efficient iterative schemes for ab initio total-energy calculations using a plane-wave basis set. *Phys. Rev. B* **1996**, *54*, 11169–11186.

(35) Wyckoff, R. W. G. *Crystal Structures*; Interscience Publishers, New York, 1963; pp 7–83.

(36) Outka, D.; Stöhr, J.; Jark, W.; Stevens, P.; Solomon, J.; Madix, R. Orientation and bond length of molecular oxygen on Ag (110) and Pt (111): A near-edge x-ray-absorption fine-structure study. *Phys. Rev. B* **1987**, *35*, 4119–4122.

(37) Henkelman, G.; Uberuaga, B. P.; Jónsson, H. A climbing image nudged elastic band method for finding saddle points and minimum energy paths. *J. Chem. Phys.* **2000**, *113*, 9901–9904.

(38) Johnson, C. L.; Snoeck, E.; Ezcurdia, M.; Rodríguez-González, B.; Pastoriza-Santos, I.; Liz-Marzán, L. M.; Hÿtch, M. J. Effects of elastic anisotropy on strain distributions in decahedral gold nanoparticles. *Nat. Mater.* **2008**, *7*, 120–124.

(39) Amano, F.; Prieto-Mahaney, O.-O.; Terada, Y.; Yasumoto, T.; Shibayama, T.; Ohtani, B. Decahedral single-crystalline particles of anatase titanium (IV) oxide with high photocatalytic activity. *Chem. Mater.* **2009**, *21*, 2601–2603.

(40) Walsh, M. J.; Yoshida, K.; Kuwabara, A.; Pay, M. L.; Gai, P. L.; Boyes, E. D. On the structural origin of the catalytic properties of inherently strained ultrasmall decahedral gold nanoparticles. *Nano Lett.* **2012**, *12*, 2027–2031.

(41) McKenna, K. P. Gold nanoparticles under gas pressure. *Phys. Chem. Chem. Phys.* **2009**, *11*, 4145–4151.

(42) Barnard, A. S.; Curtiss, L. A. Predicting the shape and structure of face-centered cubic gold nanocrystals smaller than 3 nm. *ChemPhysChem* **2006**, *7*, 1544–1553.

(43) Zhang, X.; Lu, G. Computational design of core/shell nanoparticles for oxygen reduction reactions. *J. Phys. Chem. Lett.* **2013**, *5*, 292–297.

(44) Inderwildi, O. R.; Lebiedz, D.; Deutschmann, O.; Warnatz, J. Coverage dependence of oxygen decomposition and surface diffusion on rhodium (111): A DFT study. *J. Chem. Phys.* **2005**, *122*, 034710.

(45) Ashcroft, N. W.; Mermin, N. D. *Solid State Physics*; Holt, Rinehart, and Winston, New York, 1976; Chapter 7, p 123.

(46) Wang, C. M.; Baer, D. R.; Thomas, L. E.; Amonette, J. E.; Antony, J.; Qiang, Y.; Duscher, G. Void formation during early stages of passivation: Initial oxidation of iron nanoparticles at room temperature. *J. Appl. Phys.* **2005**, *98*, 094308.

(47) Burdett, J. K.; Hughbanks, T.; Miller, G. J.; Richardson Jr, J. W.; Smith, J. V. Structural-electronic relationships in inorganic solids: powder neutron diffraction studies of the rutile and anatase polymorphs of titanium dioxide at 15 and 295 K. *J. Am. Chem. Soc.* **1987**, *109*, 3639–3646.

(48) Charlton, G.; Howes, P.; Nicklin, C.; Steadman, P.; Taylor, J.; Muryn, C.; Harte, S.; Mercer, J.; McGrath, R.; Norman, D. et al. Relaxation of $TiO_2$ (110)-(1$\times$ 1) using surface X-ray diffraction. *Phys. Rev. Lett.* **1997**, *78*, 495–498.

(49) Janotti, A.; Varley, J.; Rinke, P.; Umezawa, N.; Kresse, G.; Van de Walle, C. Hybrid functional studies of the oxygen vacancy in $TiO_2$. *Phys. Rev. B* **2010**, *81*, 085212.

(50) Liu, J.; Fan, X.; Sun, C.; Zhu, W. Oxidation of the titanium (0001) surface: diffusion processes of oxygen from DFT. *RSC Adv.* **2016**, *6*, 71311–71318.

# 8 TOC Graphic